

A Geometrical Approach for Solving 2D Eikonal Equation

C. K. Au¹

Abstract: Solving the Eikonal equation is popular due to its potential applications in various areas. Numerical method is the most common approach to solve the equation. This paper presents a geometric approach to solve the equation. Each point in a two dimensional domain with a given velocity field is characterized by the least time from the source. The path of least time is obtained by the Euler equations characterizing the extrema of the variation problem. A geometric representation of the space time function for the source is constructed. The solution to the eikonal equation is obtained based on space time geometry.

keyword: path of least time, eikonal equation, front propagation

1 Introduction

The Eikonal equation describes the time propagation in a given velocity field. Due to its numerous applications [Sethian (1999b), Lions (1982), Bardi and Copnzzo-Dolectta (1997), Osher and Fedkiw (2003), Qian and Symes (2001), Cheng, Kang, Osher, Shim, and Tsai (2004)], solving the equation is an active topic of research. The equation may be solved analytically in certain situations; however, numerical methods have been recognized as the most efficient means of the computation since the velocity field and the existence of obstacles complicate the propagation. Among the various algorithms [Mauch (2003), Reitich and Tamma (2004)] proposed to solve the equation, fast marching method [Mauch (2003), Sethian (1999a), Sethian and Vladimirsky (2000)], level set methods [Sethian (1999b), Kim (2001), Adalsteinsson and Sethian (1999), Barth and Sethian (1998)] and fast sweeping method [Tsai, Cheng, Osher, and Zhao (2003), Kao, Osher, and Qian (2003), Zhao (2004)] are three popularly adopted approaches. For a given velocity field with obstacles, two

major phases are included in these approaches: *discretization of the flow field* and *resolution of the nonlinear discrete system*. The discrete domain can be a structured or an unstructured mesh. The obstacles are considered as the regions with zero speed in the velocity field. Finite difference method is used to solve the system of equations obtained from the mesh.

This paper presents a geometric approach to solve the two dimensional Eikonal equation. A flow path from a primary source is determined by a given static velocity field which is a function of the location in the two dimension domain. Secondary sources are activated as the flow collides with the obstacles. These secondary sources complicate the flow pattern. A space time function is adopted to describe the flow from each source, either primary or secondary. These functions are represented by a set of solid geometries [Mantyla (1988)]. The resultant space time function is created by Boolean sum [Mantyla (1988)] of these geometries. The flow fronts are determined from this solid geometry.

2 Eikonal Equation

The 2D eikonal equation for describing the propagation time $t(x_1, x_2)$ from a primary source Γ_i to a point (x_1, x_2) has the form of

$$\begin{aligned} v|\nabla t| &= 1 & \text{in } \Omega \subset \mathbf{R}^2 \\ t &= 0 & \text{on } \Gamma_i \subset \mathbf{R}^2 \end{aligned} \quad (1)$$

where $v = v(x_1, x_2)$ is a velocity field; Ω is the 2D computational domain.

A flow path γ in the Euclidean domain \mathbf{R}^2 is given by a vector-valued function of the path length s defined on some interval $[a, b]$

$$\gamma(s) = ((x_1(s), x_2(s)))$$

Denoting $y_{,k} = \frac{dy}{dx_k}$ ($\forall k = 1, 2$) and $y_{,s} = \frac{dy}{ds}$ as the first derivative of y with respect to x_k and s respectively.

¹ School of Mechanical and Aerospace Engineering, Nanyang Technological University, Singapore

Lemma 0. The flow path between two points in a 2D Euclidean domain satisfies the Eikonal equation.

Proof. Use chain rule, $x_{k,s} = \frac{1}{v}x_{k,t}$ which implies

$$t_{,k} = \frac{1}{v}s_{,k}$$

As a result,

$$\sum t_{,k}^2 = \frac{1}{v^2} \sum s_{,k}^2$$

Since $s = \sqrt{g_{ij}x^i x^j}$ in the 2D Euclidean domain,

$$s_{,k} = \frac{x_k}{\sqrt{g_{ij}x^i x^j}}$$

Hence

$$t_{,1}^2 + t_{,2}^2 = \frac{1}{v^2}$$

or

$$v|\nabla t| = 1$$

□

Equation (1) is nonlinear. The nonlinearity is essential for producing multiple branches of solution. Multiple branches include various modes of propagation such as reflection, refraction and diffraction. Multiple paths also exist in each mode. Different paths between two points **p** and **q** are shown in figure 1.

Given a path parametrized in u , with components its *line element* $(ds)^2 = g_{ij}dx^i dx^j$ is invariant. As it will be useful, the conversion factor between the parameter u and the arc length s is:

$$ds = \sqrt{g_{ij}(x^i_{,u})(x^j_{,u})} du \tag{2}$$

Among the multiple paths for the eikonal equation, the path of least time is adopted. The geometry of the path γ in a 2D Euclidean domain \mathbf{R}^2 is affected by two factors:

1. the velocity field and;
2. the obstacles in the domain.

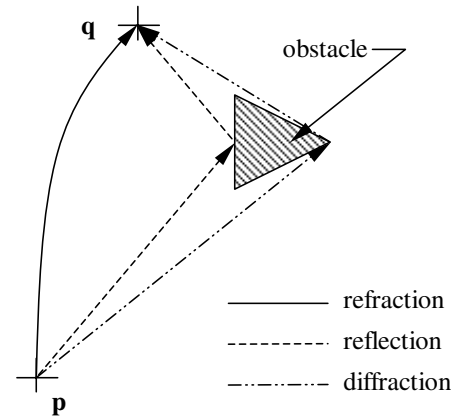


Figure 1 : Multiple paths between two points

3 Path Curvature Due to Velocity Field

The time of travel t along a path γ_{ab} from **a** to **b** with speed v is given as

$$t = \int_{\gamma_{ab}} \eta ds \tag{3}$$

where $\eta = \frac{1}{v}$ is also known as slowness field.

The calculus of variation allows one obtain a differential equation for describing the path that has least travel time between two points. Differentiating the functional (3) invokes the necessary condition of the *Euler-Lagrange* equations:

$$f_{,i} = \frac{d}{du} \left(\frac{\partial f}{\partial x_{i,u}} \right) \forall i = 1, 2 \tag{4}$$

where

$$f = \eta \sqrt{g_{ij}(x^i_{,u})(x^j_{,u})}$$

If the conversion equation (2) between du and ds is unity,

$$s_{,u} = \sqrt{g_{ij}(x^i_{,u})(x^j_{,u})} = 1$$

then the following result is immediate.

Lemma 1. The flow path between two points in a 2D Euclidean domain involves the solution of the Euler-Lagrange equations in the form:

$$\nabla \eta = \frac{d(\eta \mathbf{x}')}{ds} \tag{5}$$

where $\mathbf{x}' = (x_{1,s}, x_{2,s})$.

Proof. Verification of the x_1 -component proceeds as follows. Since $\sqrt{g_{ij}(x_{1,u}^i)(x_{1,u}^j)} = 1$ implies $u = s$ and $f = \eta$. Therefore,

$$\frac{\partial f}{\partial x_1} = \frac{\partial \eta}{\partial x_1}$$

and

$$\frac{d}{du} \left(\frac{\partial f}{\partial x_{1,u}} \right) = \frac{d}{du} \left(\frac{\partial \left(\eta \sqrt{g_{ij}(x_{1,u}^i)(x_{1,u}^j)} \right)}{\partial x_{1,u}} \right)$$

which gives

$$\frac{d}{du} \left(\frac{\partial f}{\partial x_{1,u}} \right) = \frac{d}{ds} (\eta x_{1,u})$$

Hence,

$$\frac{\partial \eta}{\partial x_1} = \frac{d}{ds} (\eta x_{1,s})$$

Expanding equation (5) yields

$$\mathbf{x}'' = \mathbf{x}' \times (\nabla \ln \eta \times \mathbf{x}') \quad (6)$$

Hence, the propagation path will be a straight line for constant speed. Curvature is introduced into the path if the speed is not a constant in the domain, which implies the introduction of forces. For instance, if the speed $v = kx_2$ (i.e. speed is proportional to the x_2 co-ordinate), the path takes on the form of a circular arc in \mathbf{R}^2 . Similarly, if $v = \frac{k}{x_2}$ (i.e. speed is inversely proportional to the x_2 co-ordinate), the flow path will be a catenary.

4 Path Curvature Due to Obstacles

The obstacles in the domain are symbolized by a set of boundaries. A more detail discussion of the geometric definition of an obstacle can be found in reference [Angluin, Westbrook, and Zhu (2001)]. When an obstacle exists and blocks the path, a path of local minimal time of travel will be picked. As a result, the path goes around the obstacle.

For the existence of an obstacle, the 2D Euclidean domain \mathbf{R}^2 is divided into two regions, \mathbf{R}_i (the region which is inside the obstacle) and \mathbf{R}_o (the region which is outside the obstacle) by a closed boundary $\partial \mathbf{R}$.

Definition 1. A *concave* boundary is a part of a closed boundary which is concave to a region.

Definition 2. A *convex* boundary is a part of a closed boundary which is convex to a region.

Hence, a concave boundary to the region \mathbf{R}_i is a convex boundary to the region \mathbf{R}_o .

Lemma 2. If the path of least time γ_{ab} between two points \mathbf{a} and \mathbf{b} in a 2D Euclidean region \mathbf{R}_o is blocked by the boundary (i.e. it intersects the concave boundary segment $\partial \mathbf{R}$ so that the path is partially in the region \mathbf{R}_i), then the flow path γ'_{ab} is expressed as

$$\gamma'_{ab} = \gamma_{at_1} \cup \partial \mathbf{R}_{t_1 t_2} \cup \gamma_{t_2 b}, \forall \gamma_{at_1}, \partial \mathbf{R}_{t_1 t_2}, \gamma_{t_2 b} \subset \mathbf{R}_o$$

where \mathbf{t}_1 and \mathbf{t}_2 are points on $\partial \mathbf{R}$ which are tangent to γ_{at_1} and $\gamma_{t_2 b}$ respectively;

$\partial \mathbf{R}_{t_1 t_2}$ is part of $\partial \mathbf{R}$ with two extreme points \mathbf{t}_1 and \mathbf{t}_2 and is concave to the region \mathbf{R}_o .

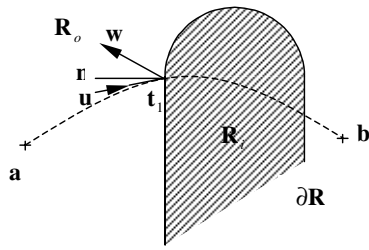
Proof. Figure 2(a) shows a part of a boundary $\partial \mathbf{R}$ and the corresponding two regions. Let \mathbf{u} and \mathbf{w} be the incident and reflected velocity respectively. Considering the assumption of no reflection and conservation of momentum, $\mathbf{u} \cos \theta = \mathbf{0}$ and $\mathbf{u} \sin \theta = \mathbf{w} \sin \phi$ where θ and ϕ are the incident angle and reflected angle with the normal vector \mathbf{n} at \mathbf{t}_1 . $\mathbf{u} \neq \mathbf{0}$ implies $\theta = \frac{\pi}{2}$ and $\mathbf{u} = \mathbf{w}$ (since $\theta = \phi$). Hence, γ_{at_1} is tangent to $\partial \mathbf{R}_{t_1 t_2}$ at \mathbf{t}_1 . Similarly, $\gamma_{t_2 b}$ is tangent to $\partial \mathbf{R}_{t_1 t_2}$ at \mathbf{t}_2 as shown in figure 2(b). Therefore, $\gamma_{at_1} \cup \partial \mathbf{R}_{t_1 t_2} \cup \gamma_{t_2 b}$ is the path within the region \mathbf{R}_o . \square

Corollary 2.1 If the boundary segment $\partial \mathbf{R}_{cd}$ is both concave and convex, then the flow path $\gamma'_{a'b'}$ is expressed as

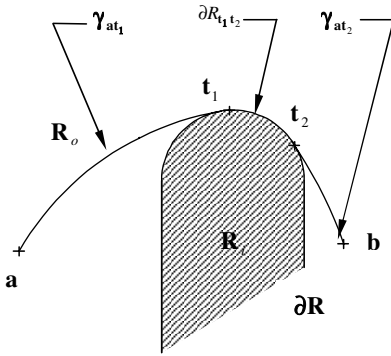
$$\gamma'_{a'b'} = \gamma_{a't'_1} \cup \partial \mathbf{R}_{t'_1 t'_2} \cup \gamma_{t'_1 t'_2} \cup \partial \mathbf{R}_{t'_2 t'_2} \cup \gamma_{t'_2 b'} \\ \forall \gamma_{a't'_1}, \partial \mathbf{R}_{t'_1 t'_2}, \gamma_{t'_1 t'_2}, \partial \mathbf{R}_{t'_2 t'_2}, \gamma_{t'_2 b'} \subset \mathbf{R}_o$$

where \mathbf{t}'_1 and \mathbf{t}'_2 are points on $\gamma_{t'_1 t'_2}$ which are tangent to $\partial \mathbf{R}$.

Proof. Figure 3 shows a combination of two situations described by Lemma 2. Setting point $\mathbf{a}' = \mathbf{a}$, $\mathbf{t}'_2 = \mathbf{b}$, by



(a) obstacle on the path of least time between a and b



(b) the path between a and b

Figure 2 : The propagation path around an obstacle

Lemma 2, implies that t'_1 is a tangent point on $\Gamma_{t_1 t'_1}$. Similarly, setting $b' = b$, $t'_1 = a$ indicates that t'_2 is a tangent point on $\partial R_{t'_2 t_2}$. Therefore $\gamma_{t'_1 t'_2}$ is tangent to the concave boundary segments $\partial R_{t_1 t'_1}$ and $\partial R_{t'_2 t_2}$ \square

Corollary 2.2 If there exists a *reentrant vertex* v on the boundary of the region R_o which blocks the path of least time γ_{ab} between two points a and b , then the flow path γ'_{ab} is expressed as

$$\gamma'_{ab} = \gamma_{av} \cup \gamma_{vb}, \forall \gamma_{av}, \gamma_{vb} \subset R_o$$

Proof. Figure 4(a) depicts the flow path between two points. Due to the existence of the concave boundary, the deflected flow path $\gamma'_{ab} = \gamma_{at_1} \cup \partial R_{t_1 t_2} \cup \gamma_{t_2 b}$ as specified by **Lemma 2**. If the concave boundary degenerates to a reentrant vertex v as shown in figure 4(b) (t_1 and t_2 converge to v), then the flow path becomes $\gamma'_{ab} = \gamma_{av} \cup \gamma_{vb}$. \square

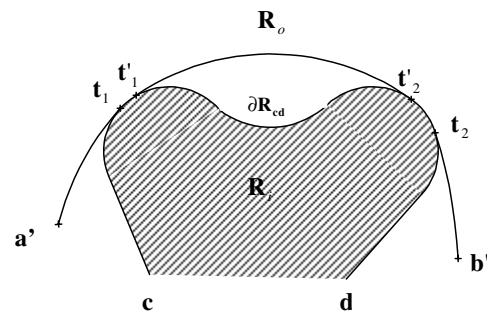
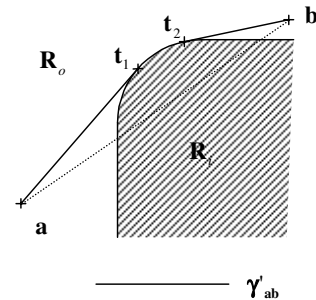
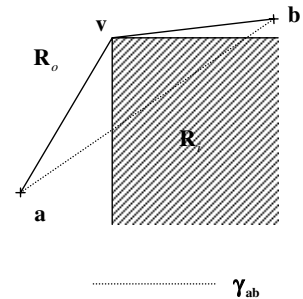


Figure 3 : The propagation path along a boundary segment



(a) a concave boundary



(b) a reentrant vertex on a boundary

Figure 4 : Flow path over a reentrant vertex

5 Space Time Geometry of a Source

A *source* emits continuously in the region. Hence, the flow paths start at the source.

Definition 3. A source Γ_i is a geometric entity $\Gamma_i \subset \mathbf{R}^2$ such that the flow path is $\gamma_{sb}, \forall s \in \Gamma_i$ and $\forall b \in \mathbf{R}^2$.

A source can be further categorized into *point source*, *curve source* and *region source* based on the geometric

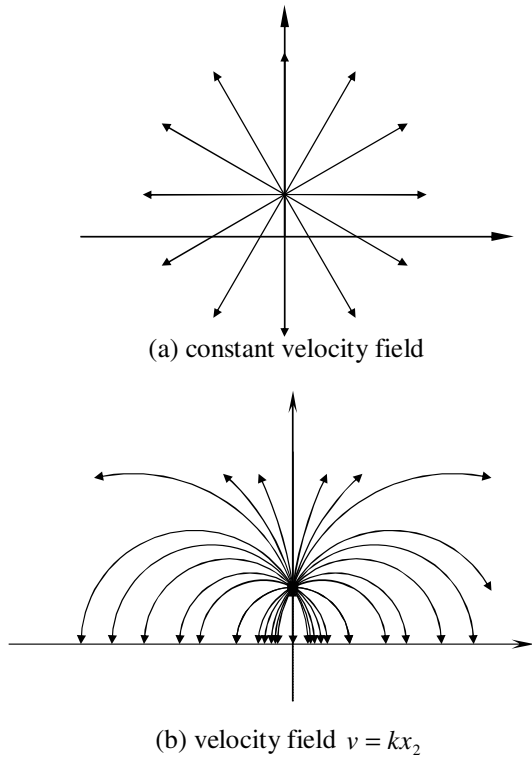


Figure 5 : Propagation paths from a point source with different velocity field

entity.

Figure 5(a) and 5(b) show the flow paths from a point source with constant speed and speed proportional to the axis x_2 respectively.

The flow front from an emitted point source is the front line of the emission. It is a topological circle in the domain. An advancing flow front is a function of time t . The flow front possesses the geometrical property that it must be *orthogonal* to the flow path from the source.

Lemma 3. The Euler-Lagrange equations for a flow path of least time adopt the form:

$$\ddot{x}_i = \lambda_i^j (\ln \eta)_{,j} \quad (7)$$

$$\text{where } \lambda_i^j = \left(\frac{\delta_{ij}}{\eta^2} - 2\dot{x}_i \dot{x}_j \right) (\ln \eta)_{,j}$$

Proof. Form equation (6),

$$\frac{d^2 x_i}{ds^2} = \sum_j \left(\delta_{ij} - \frac{dx_i}{ds} \frac{dx_j}{ds} \right) (\ln \eta)_{,j}$$

Rewriting as

$$\begin{aligned} & \frac{dt}{ds} \frac{d}{dt} \left(\frac{dx_i}{ds} \right) \\ &= \sum_j \left(\delta_{ij} - \left(\frac{dt}{ds} \right) \left(\frac{dx_i}{dt} \right) \left(\frac{dt}{ds} \right) \left(\frac{dx_j}{dt} \right) \right) (\ln \eta)_{,j} \end{aligned}$$

Substituting $\frac{dt}{ds} = \eta$ gives

$$\eta \frac{d}{dt} (\eta \dot{x}_i) = \sum_j (\delta_{ij} - \eta^2 \dot{x}_i \dot{x}_j) (\ln \eta)_{,j}$$

Expanding the left hand side yields

$$\eta (\dot{\eta} \dot{x}_i + \eta \ddot{x}_i) = \sum_j (\delta_{ij} - \eta^2 \dot{x}_i \dot{x}_j) (\ln \eta)_{,j}$$

Since $\dot{\eta} = \eta_{,k} \dot{x}^k$ which implies

$$\eta (\eta_{,j} \dot{x}^j \dot{x}_i + \eta \ddot{x}_i) = \sum_j (\delta_{ij} - \eta^2 \dot{x}_i \dot{x}_j) (\ln \eta)_{,j}$$

Re-arrangement of the terms yields $\ddot{x}_i = \lambda_i^j (\ln \eta)_{,j} \quad \square$

Figure 6 shows the flow fronts of the point sources corresponding to that in figure 5.

A *space time* describes the position in domain with a velocity field v at a specific time instant. **Lemma 3** gives the relationship between a two dimensional space (in terms of x_1, x_2) and time in terms of the direction of flow at the source.

Definition 4. The space time function of a source \mathbf{j} is defined as $\Psi_j : E^2 \rightarrow R$ such that $t = \Psi_j(x_1, x_2), \forall t \in R, (x_1, x_2) \in E^2$ and $\dot{x}_i = \lambda_i^j (\ln \eta)_{,j}$ with the initial condition $(x_1(t_0), x_2(t_0)) \in \mathbf{j}$.

Hence, the space time function Ψ_j of a source \mathbf{j} at $(0, y_0)$ in a velocity field $v = k$ and $v = kx_2$ (where k is a constant) are given by equation (7) in implicit form of:

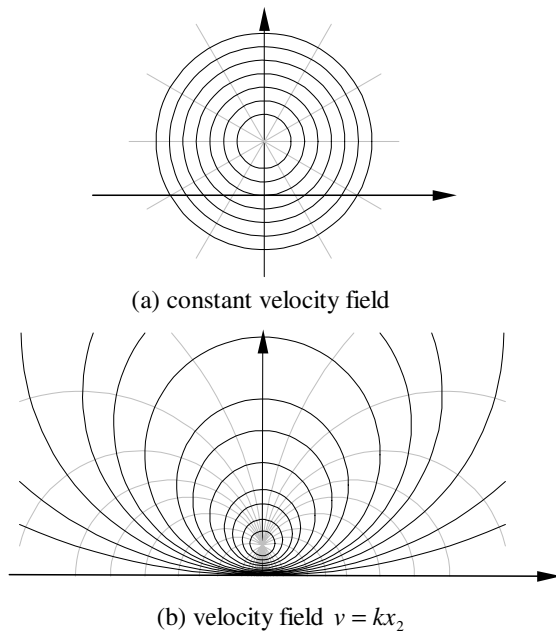
$$(x_1)^2 + (x_2 - y_0)^2 = k^2(t_j - t)^2 \quad (8)$$

and

$$(x_1)^2 + \left(x_2 - y_0 \frac{e^{2k(t-t_j)} + 1}{e^{k(t-t_j)}} \right)^2 = \frac{y_0^2}{4} \left(\frac{e^{2k(t_j-t)} - 1}{e^{k(t_j-t)}} \right)^2 \quad (9)$$

where t_j is the time delay of source \mathbf{j} .

Figure 7 shows space time function of a point source \mathbf{j} at $(0, y_0)$ in a constant speed field with a time delay t_j . The



————— flow fronts ———— flow path

Figure 6 : Flow fronts from a point source with different velocity field

black curves link all the *events* happen simultaneously while the grey lines are the *world lines*.

The space time function of a point source \mathbf{j} at $(0, y_0)$ in a velocity field $v = kx_2$ with a time delay $t_j = 0$ is plotted in figure 8.

A curve source \mathbf{c} is considered as an aggregation of infinite number of point sources along the curve. All these point sources co-operate to acquire territories. The space time function of the curve source is given as:

$$\Psi_{\mathbf{c}}(x_1, x_2) = \min[\Psi_{\mathbf{j}}(x_1, x_2)], \forall \mathbf{j} \in \mathbf{c}, \forall (x_1, x_2) \in \mathbf{R}^2 \quad (10)$$

Hence, the space time function of a curve source is the envelope obtained by sweeping the space time function of a point source with time delays. Figure 9(a) and 9(b) show the space time functions of a line and a curve source with various time delay in a domain with a constant speed field respectively, while figure 9(c) is the space time function of a line source with constant time delays along the source in a domain with velocity field $v = kx_2$. Similarly, the space time function of a region source \mathbf{p} with constant speed field is shown in figure 9(d).

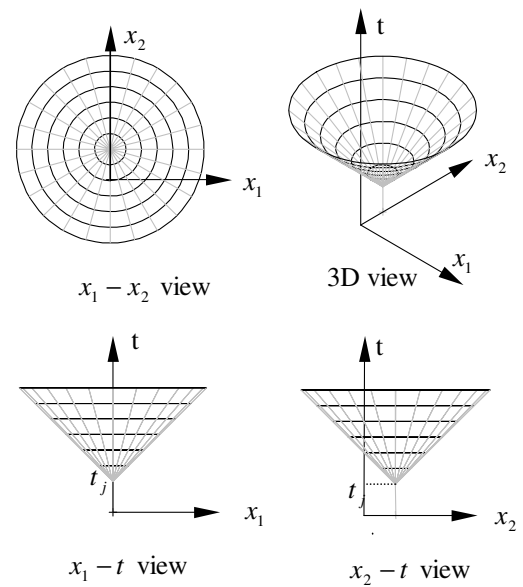


Figure 7 : Space time function of a point source in a constant velocity field

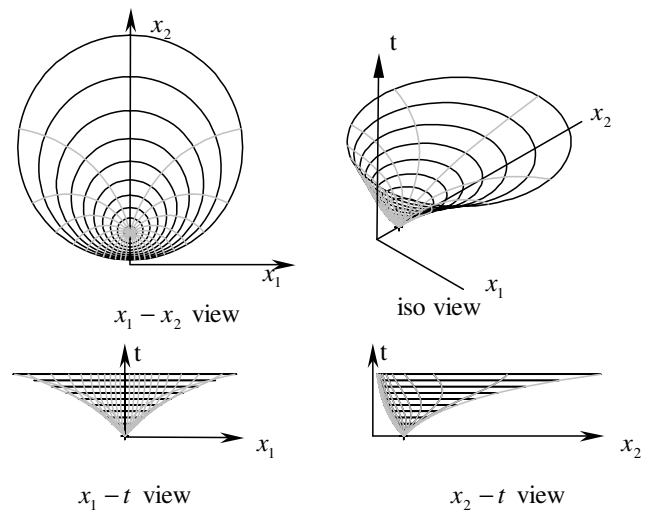


Figure 8 : Space time function of a point source in a velocity field $v = kx_2$

6 Source and Obstacles

Consider a source \mathbf{j} in a 2D Euclidean domain with a boundary. If the boundary is convex, the flow paths from the source will only be deflected due to the change of flow velocity as specified in **Lemma 1**. However, if the boundary is concave, then certain areas within the

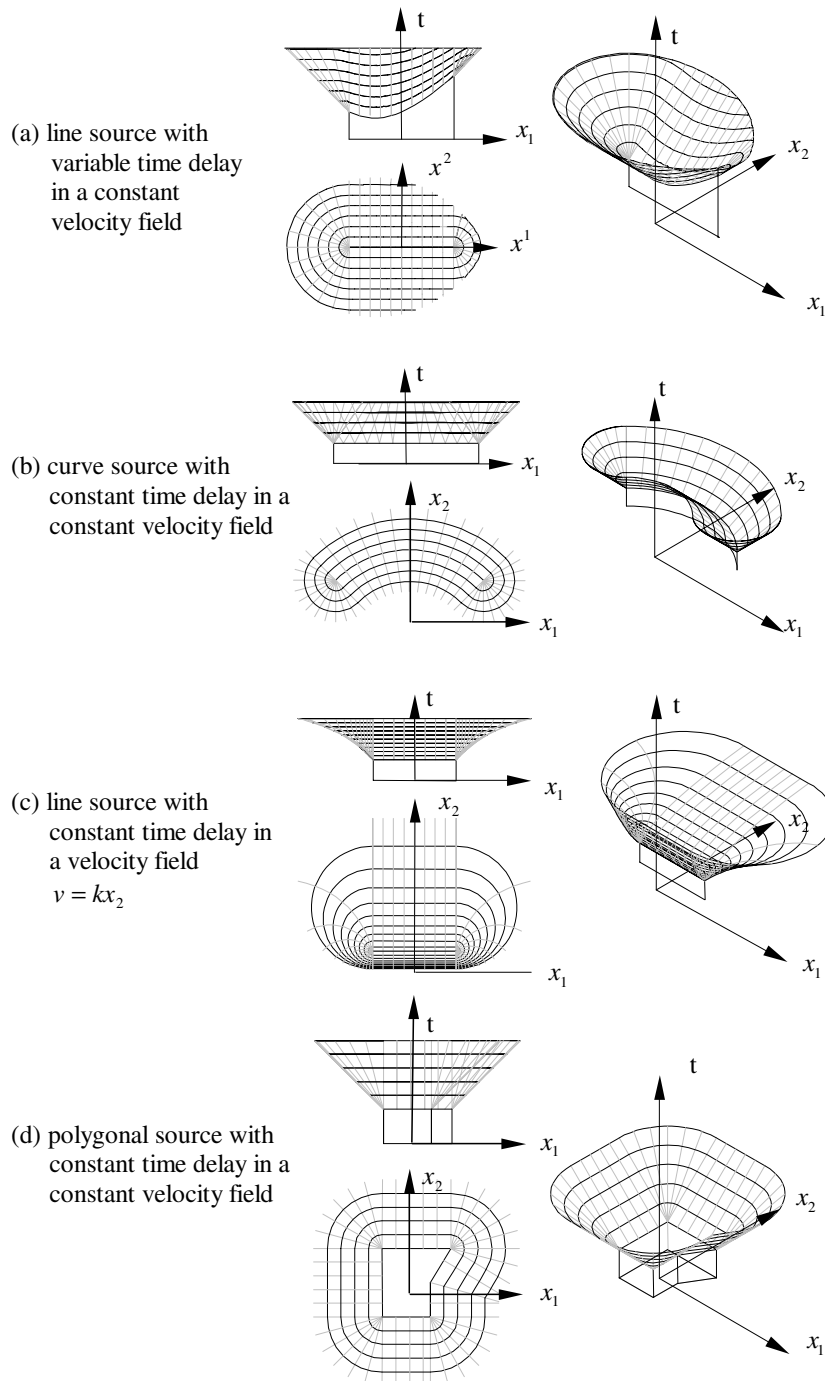


Figure 9 : Various curve sources

boundary will be shielded by the concave segment of the boundary. By **Lemma 2**, the flow paths between any locations in these areas and the source will be tangent to the concave boundary segment. A set of flow paths in a bounded 2D Euclidean domain with constant speed field

is plotted in figure 10(a). The domain is partitioned into two regions: the “light grey” region with straight flow path from the source \mathbf{j} as the velocity is constant, while the flow paths (from the source \mathbf{j}) in the “dark grey” region are deflected due to the concave boundary seg-

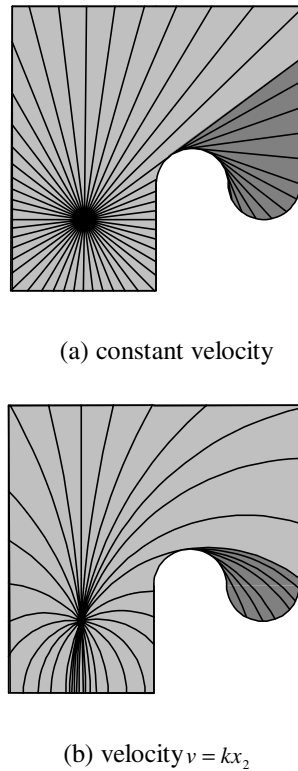


Figure 10 : Propagation paths in a domain with boundary

ment. Figure 10(b) gives a similar plot with flow velocity $v = kx_2$. The flow paths from the source \mathbf{j} to the “dark grey” region are deflected by both speed variation and obstacle.

Focusing on the “dark grey” region reveals that all the flow paths in this region originate from the concave segment of the boundary as illustrated in figure 11. This segment starts at the tangent point \mathbf{p} between the flow path from \mathbf{j} and the boundary, and ends at the point of inflection \mathbf{q} on the boundary. As a result, this segment is considered as a *secondary source* in the “dark grey” region. This secondary source is a curve source with variable time delay. The delay is the time of travel from the source \mathbf{j} to various points on the source.

7 Flow Pattern Generation by Geometric Approach

Flow pattern is important in describing the propagation from a primary source in a domain since it tells the complexity of the propagation.

Definition 5. A flow pattern from a source in a domain is an aggregation of the flow fronts.

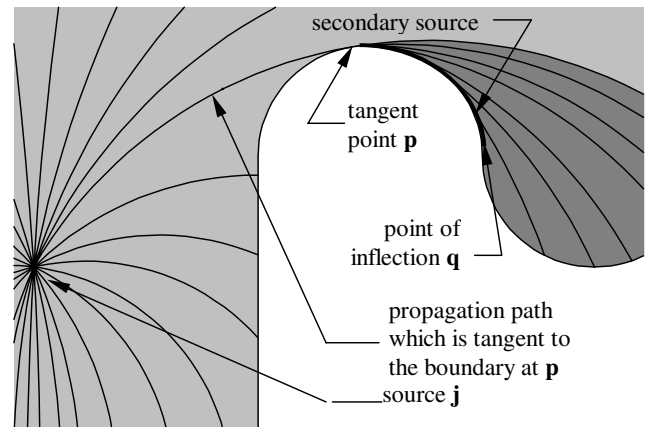


Figure 11 : A secondary source

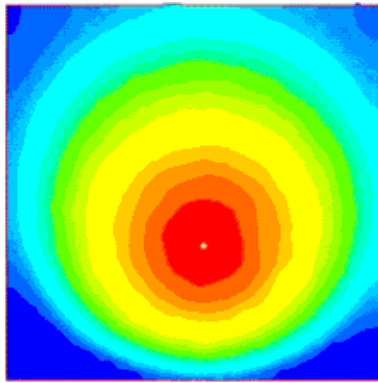
Figure 12(a) illustrates the flow pattern from a primary point source with space time function as shown in figure 8. (As the commercial software is intended for plastic mold injection, the thickness of the molding is made to vary with the x_2 -axis so as to simulate a velocity field with $v = kx_2$.) The flow pattern are computed and shown in figure 12(b).

Since the flow paths are deflected (and hence the flow fronts are distorted) by the flow velocity variation and the boundaries, the flow pattern from a source in a bounded domain with obstacles can be complicated. As secondary sources may arise in a domain due to the geometry of the boundary (and the obstacles), a resultant space time function from a source is obtained by composing the space time functions from various sources (including the secondary sources). The flow pattern can be obtained from the space time function of a source.

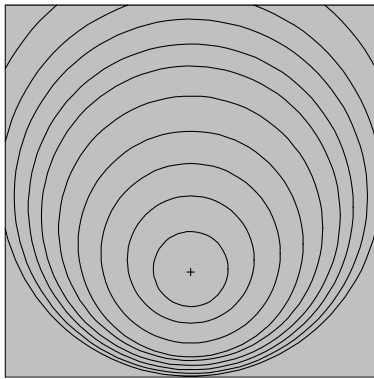
A geometric approach is proposed to construct the flow pattern.

Secondary sources identification For a two dimensional domain, there are two types of secondary sources arise when the flow propagates around an obstacle: curve source and point source. A secondary source is a curve source if there is a flow path of least time which is tangent to the boundary (either domain boundaries or obstacle boundaries). The source starts at the tangent point and ends at either a point of inflection or another source. A point source arises when there is a reentrant vertex on the (domain or obstacle) boundary.

Solid geometry creation A solid geometry K_j for each



(a) numerical solution



(b) closed form solution

Figure 12 : Flow pattern of a point source in a velocity field with $v = kx_2$

source \mathbf{j} (including secondary sources) is defined to represent the space time function given in **definition 4** as

$$\mathbf{K}_j = \{ (x_1, x_2, t) | t_\infty > t \geq \Psi_j(x_1, x_2) \geq 0; \forall (x_1, x_2) \in E^2 \wedge t \in \mathbf{R} \}$$

where t_∞ is the upper bound of the time t .

Definition 4 is defined with a monotonic increasing time variable t . If this space time function is geometrized, an upper bound of t , denoted by t_∞ , is needed to obtain an finite solid geometry.

Resultant space time function creation Since the resultant space time function of multiple sources is $\Psi_c(x_1, x_2) = \min[\Psi_j(x_1, x_2)], \forall \mathbf{j} \in \mathbf{c}, \forall (x_1, x_2) \in \mathbf{R}^2$ (as specified in equation (10)), the solid geometry representing the resultant space time function is the boolean sum of all these

solid geometries:

$$\mathbf{K} = \bigcup_j \mathbf{K}_j \quad (11)$$

Sectioning and projection Sectioning the solid geometry \mathbf{K} with a set of planes $t \geq 0$ gives the flow fronts at the time instant t . Projecting these flow fronts onto the space $(x_1 - x_2)$ plane) gives the flow pattern in a 2D Euclidean domain.

8 Examples

Three examples are listed to show the propagation of the flow front. In order to compare the flow patterns, the solution for each example is shown with a similar plot from a commercial finite element flow analysis.

Example 1: Flow pattern from a primary source in constant velocity field with a circular obstacle

Figure 13 shows an example of flow pattern generation by geometric approach. Consider a rectangular two dimensional domain with a circular obstacle. Assuming that the flow speed is constant for simplicity, hence the solid geometry representing the space time function is a solid cone. The time axis is pointing downward for easy visualization. Two curve secondary sources are identified in the domain with time delay. In figure 13(a), the domain is partitioned into two regions: “light grey” region is filled up by the source \mathbf{j} while the “dark grey” region is covered by the secondary sources. Figure 13(b), 13(c) and 13(d) show the solid cones representing the space time functions of source \mathbf{j} and two secondary sources. The cones are trimmed due to the domain boundaries. The Boolean sum of all the solid geometries is shown in figure 13(e). Sectioning the resultant solid geometry and projecting the section curves on the 2D domain give the flow pattern as illustrated in figure 13(f) and 13(g).

Figure 14 shows the flow pattern obtained by using finite element approach for comparison. The flow pattern basically agrees with that generated by the geometric approach.

Example 2: Flow pattern from a primary source in velocity field $v = kx_2$ (velocity is proportional to the x_2 axis) with a triangular obstacle

Figure 15(a) shows the flow pattern from a source with velocity field $v = kx_2$ (the flow velocity is inversely proportional to the x_2 axis). The flow path is a circular arc with centre on the x_1 axis. A triangular obstacle is inside the flow field. Secondary sources arise as the flow

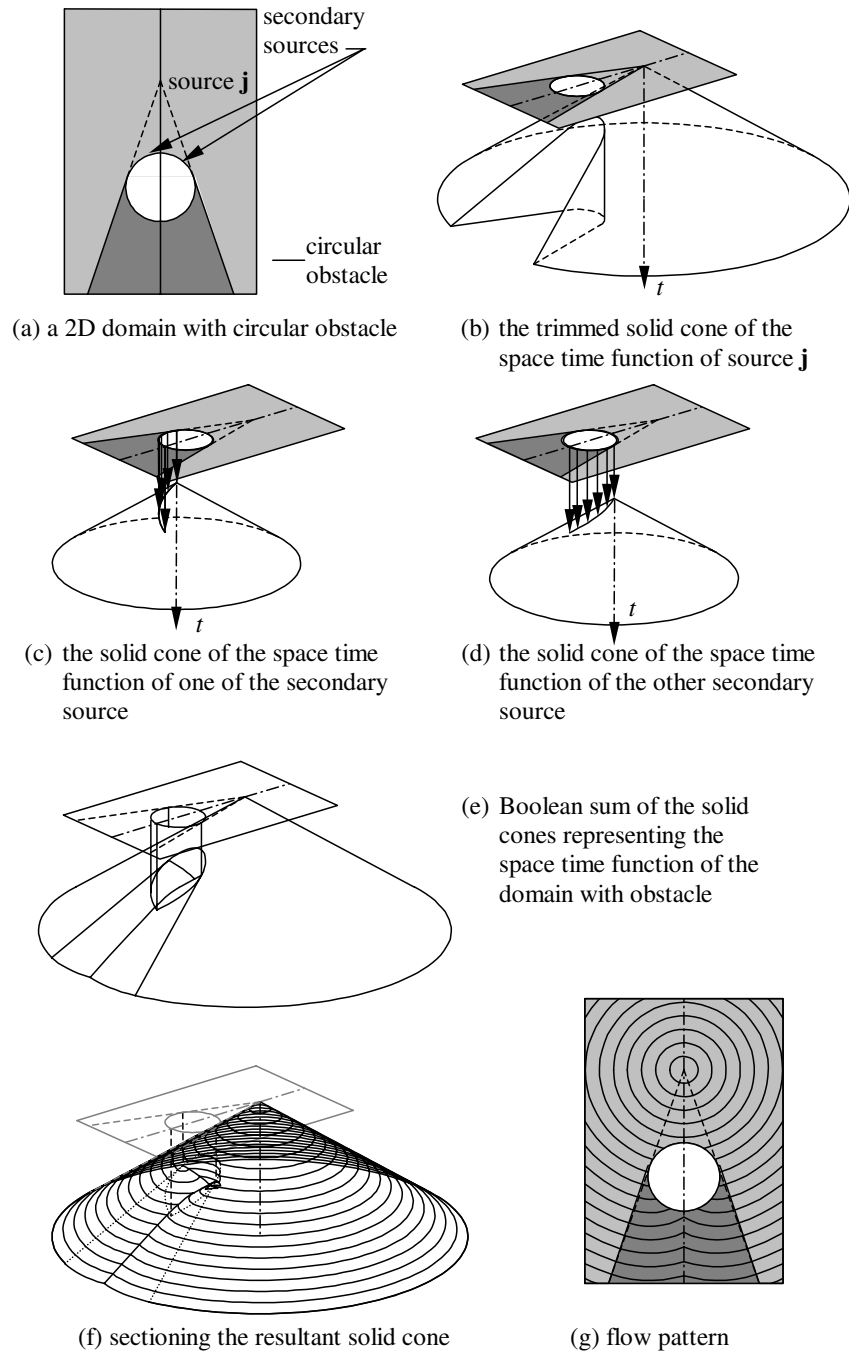


Figure 13 : Flow pattern in a constant velocity field with a circular obstacle

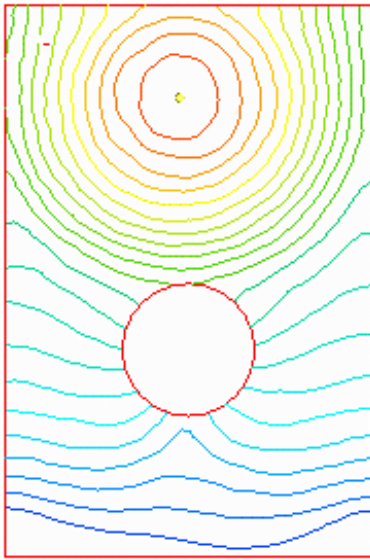


Figure 14 : Flow pattern around a circular obstacle generated by finite element method

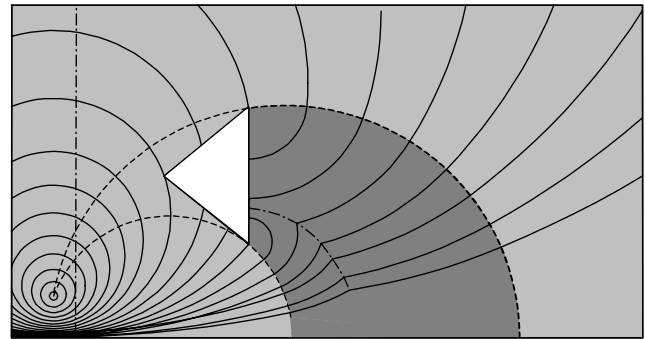
reaches the obstacle. The similar flow pattern generated by finite element method is shown in figure 15(b).

Example 3: Flow pattern from a primary source in a circular maze with constant velocity field.

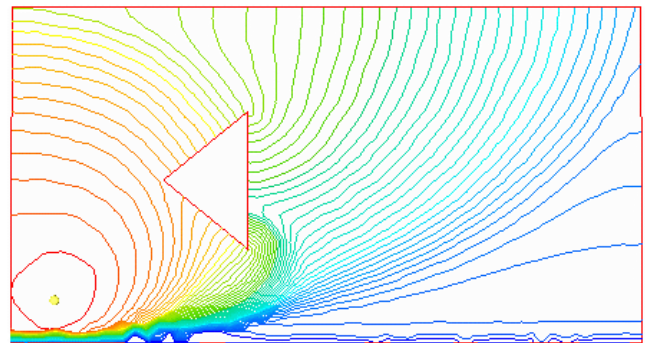
A circular maze is used to depict the flow pattern generated by geometric approach. The flow pattern is shown in figure 16. A similar result can be found in reference [Gremaud and Kuster (2004)], which is generated by fast marching method and fast sweeping method. The source is at the lower left corner with a constant velocity field. The flow is deflected due to diffraction as it propagates through the maze into the centre.

9 Discussion

Front propagation governed by the Eikonal equation is common in many physical and engineering phenomena. Certain simple situations yields complicated flow pattern. Example 1 gives a simple situation: a primary point source in a constant velocity field with a circular obstacle. The space time function of such a source is represented by a linear solid cone, the resultant space time function becomes non-linear as the flow propagates around the obstacle. Hence, a concentric circular flow pattern is transformed into a non-linear flow pattern. This is an example of giving a non-linear effect by the interaction between linear elements. Example 3 is basically



(a) flow pattern generated by geometric



(b) flow pattern generated by finite element method

Figure 15 : Flow pattern in a velocity field $v = kx_2$ with a triangular obstacle

similar to example 1 with more circular obstacles. The complexity of the flow pattern is greatly increased. A bit more complicated situation with a variable velocity field $v = kx_2$ (velocity is proportional to the x_2 axis) is shown in example 2. Rewriting the velocity field to $\frac{1}{x_2} \frac{ds}{dt} = k$ ($ds^2 = g_{ij}dx^i dx^j$) reveals that the velocity field is “constant” on a hyperbolic plane (instead of the Euclidean plane). The flow fronts are circles of Apollonius on the Euclidean plane which are “concentric circles” on the hyperbolic plane. The flow fronts in both situations are set of circular arcs with time dependent centres and radius. Comparing with the numerical approach, the proposed geometric approach gives an analytical solution for these situations.

The geometric approach for producing the flow pattern consists of four procedures:

- (i) secondary source identification;
- (ii) solid geometry creation;

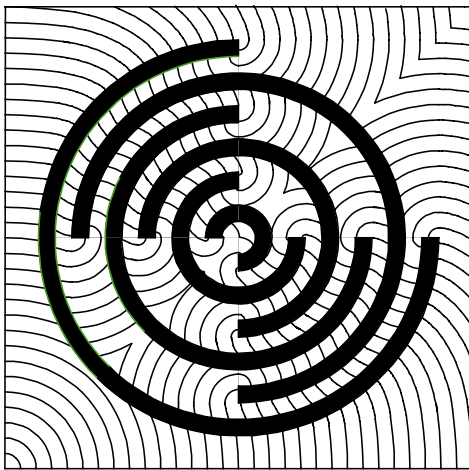


Figure 16 : Flow pattern in a circular maze with constant velocity field

- (iii) resultant space time function creation and
- (iv) sectioning and projecting.

As the complexity of the flow pattern increases exponentially with the number and the geometry of primary source, the order of the velocity field, the locations and the geometry of the obstacles, numerical methods are unavoidable, particularly for solving equation (7) to obtain the solid geometry representation for the space time function of a source. However, the efforts are greatly reduced for some common but simple situations such as the given examples if the geometric approach is adopted.

For the simple situations such as point source in constant velocity field with polygonal obstacles, secondary source identification is the common computational geometry problem of visibility graph creation. Various algorithms [Mitchell (1992), Hershberger and Suri (1999)] are available which can be adopted to identify the secondary sources. However, more exploration for an efficient algorithm to deal with the general situation of higher order geometry for the sources and obstacles, and complex dynamic velocity field $v = v(x_1, x_2, t)$ are needed in order to handle the more complicated situations.

10 Conclusion

A geometric approach is presented to solve the two dimensional Eikonal equation with a given static velocity field. It is based on the fact that secondary sources arise as the flow propagates around an obstacle. The propa-

gation is influenced by these secondary sources. Solid geometry and Boolean operation are used to model the geometry of the resultant space time function. The flow pattern, which is a solution to the Eikonal equation, is obtained from this geometrization.

The approach is particularly suitable for some common situations such as point and analytical curve sources in a constant and linear velocity field with obstacles of analytical geometry. Since only simple geometry is used by the approach in these situations, the performance is in real time because the computation involves no more algebra. These situations are common in robotics path planning, computer graphics, wave propagation etc.

References

- Adalsteinsson, D.; Sethian, J. A.** (1999): The fast construction of extension velocities in level set methods. *Journal of computational Physics*, vol. 148, pp. 2–22.
- Angluin, D.; Westbrook, J.; Zhu, W.** (2001): Robot navigation with distance queries. *siam journal of computing*. *SIAM Journal of computing*, vol. 30, no. 1, pp. 110–144.
- Bardi, M.; Copnzzo-Dolectta, I.** (1997): *Optimal control and viscosity solutions of Hamilton-Jacobi equations*. Birkhauser Boston.
- Barth, T. J.; Sethian, J. A.** (1998): Numerical schemes for the hamilton-jacobi and level set equations on triangulated domain. *Journal of computational Physics*, vol. 145, pp. 1–40.
- Cheng, L.; Kang, M.; Osher, S.; Shim, H.; Tsai, Y.** (2004): Reflection in a levelset framework for geometric optics. *CMES: Computer Modeling in Engineering & Sciences*, vol. 5, no. 4, pp. 347–360.
- Gremaud, P.; Kuster, C. M.** (2004): Computational study of fast methods for the eikonal equation. Technical Report NCSU-CRSC Tech Report CRSC-TR04-15, North Carolina State University, 2004. (<http://www4.ncsu.edu/eos/users/g/gremaud/WWW/sweepnew.pdf>).
- Hershberger, J.; Suri, S.** (1999): An optimal algorithm for euclidean shortest paths in the plane. *SIAM J. Computing*, vol. 28, no. 6, pp. 2215–2256.

- Kao, C.-Y.; Osher, O.; Qian, J.** (2003): Lax-friedrichs sweeping scheme for static hamilton-jacobi equations. *J. of Computational Physics*, vol. Article in press.
- Kim, S.** (2001): An $o(n)$ level set method for eikonal equation. *SIAM J. Sci. Comput.*, vol. 22, no. 6, pp. 2178–2193.
- Lions, P. L.** (1982): *Generalised solutions of Hamilton-Jacobi equations*. PitmanPublishing Inc. Massachusetts.
- Mantyla, M.** (1988): An introduction to solid modeling. *Computer Science Press*.
- Mauch, S.** (2003): *Efficient algorithms for solving static Hamilton-Jacobi equations*. Ph.d. dissertation, California Institute of Technology, 2003.
- Mitchell, J. S. B.** (1992): Shortest paths among polygonal obstacles in the plane. *Algorithmica*, vol. 8, pp. 55–88.
- Osher, S.; Fedkiw, R.** (2003): *Level set methods and dynamic implicit surfaces*. Springer-Verlag, New York.
- Qian, J.; Symes, W.** (2001): Paraxial eikonal solvers for anisotropic quasi-ptravel times. *Journal of computational Physics*, vol. 173, pp. 256–278.
- Reitich, F.; Tamma, K. K.** (2004): State-of-art, trends, and directions in computational electromagnetics. *CMES: Computer Modeling in Engineering & Sciences*, vol. 5, no. 4, pp. 287–294.
- Sethian, J. A.** (1999): Fast marching methods. *SIAM review*, vol. 41, pp. 195–235.
- Sethian, J. A.** (1999): *Level set methods and fast marching methods*. Cambridge UniversityPress, U.K.
- Sethian, J. A.; Vladimirovsky, A.** (2000): Fast methods for the eikonal and related hamilton-jacobi equations on unstructured meshes. *Proc. Natl. Acad. Sci. USA*, vol. 97, pp. 5699–5703.
- Tsai, Y. H. R.; Cheng, L. T.; Osher, S.; Zhao, H. K.** (2003): Fast sweeping algorithms for a class of hamilton-jacobi problems. *SIAM J. Numer. Anal.*, pp. 659–672.
- Zhao, H. K.** (2004): A fast sweeping method for eikonal equations. *mathematics of computation*. *American Mathematical Society*.

